



Red Mud as an Additive in the Extrusion of Protein-Based Porous Materials

Downloaded from: <https://research.chalmers.se>, 2026-04-16 05:46 UTC

Citation for the original published paper (version of record):

Holmström, S., Jiménez-Rosado, M., Oliver Simancas, R. et al (2025). Red Mud as an Additive in the Extrusion of Protein-Based Porous Materials. *Macromolecular Materials and Engineering*, 310(10). <http://dx.doi.org/10.1002/mame.202500052>

N.B. When citing this work, cite the original published paper.

RESEARCH ARTICLE OPEN ACCESS

Red Mud as an Additive in the Extrusion of Protein-Based Porous Materials

Saga Holmström^{1,2} | Mercedes Jiménez-Rosado³  | Rodrigo Oliver-Simancas⁴  | Amparo Jiménez-Quero⁴  | Antonio José Capezza²  | Frederico Marques Penha¹ 

¹Department of Chemical Engineering, KTH Royal Institute of Technology, Stockholm, Sweden | ²Department of Fiber and Polymer Technology, KTH Royal Institute of Technology, Stockholm, Sweden | ³Chemical Environmental and Bioprocess Engineering Group, I4 Institute, University of León, León, Spain | ⁴Division of Industrial Biotechnology, Department of Life Sciences, Chalmers University of Technology, Gothenburg, Sweden

Correspondence: Antonio José Capezza (ajcv@kth.se) | Frederico Marques Penha (frem@kth.se)

Received: 31 January 2025 | **Revised:** 1 May 2025

Funding: The authors thank Vinnova 2021-05201, Svenska Forskningsrådet Formas 2022_00362.

Keywords: protein foams | foam extrusion | porous materials | red mud | metal recovery | waste upcycling

ABSTRACT

This study explores the dual challenge of enhancing the properties of protein-based foams produced from agricultural by-products through the incorporation of red mud waste from alumina production. Foams were manufactured using an extrusion process, employing gluten and zein proteins, with raw red mud and its oxalic acid leachates serving as additives. A factorial design was utilized to assess the significance of various parameters on the mechanical properties of materials. The results indicate that red mud-based additives do not improve foam mechanical stability in terms of stiffness (as measured by Young's modulus) and thus do not function effectively to form short crosslinking bridges. However, the results show red mud serves mainly as a plasticizer and reducing/oxidizing agent, while also potentially enhancing the formation of long crosslinking bridges. This is evidenced by a significant increase in foam strain when red mud powder is extruded with gluten, reaching 190% strain at break and densities between 500 and 1500 kg/m³. Consequently, red mud shows potential to be repurposed as an additive in protein-based foams, suitable for applications requiring elastic deformation while keeping a stable porous structure manufactured via continuous extrusion.

1 | Introduction

Waste production and accumulation is a major problem in many industries, posing threats to the environment and, directly or indirectly, to human health. Estimates indicate that global solid waste generation is expected to exceed 2.5 billion metric tons by 2030, with only 20% being recycled and the remainder ending up in landfills, particularly in developing countries. Given the continuous population growth, scientific advancement, and urbanization leading to resource depletion, as well as the associated risks and costs of managing solid waste and landfills,

strategies toward achieving zero waste have been developed as the challenge is urgent [1–4].

One waste known for its massive landfilling worldwide is red mud (RM), the main waste stream generated in the industrial production of alumina from bauxite ore through the Bayer process [5–8]. Due to the heavy use of caustic soda (NaOH), the liquid phase separated from the RM slurry is highly alkaline (pH 11–13) [9, 10]. Its high alkalinity, along with the presence of potentially toxic elements, makes storage and disposal of RM a major environmental issue, causing groundwater contamination

This is an open access article under the terms of the [Creative Commons Attribution](https://creativecommons.org/licenses/by/4.0/) License, which permits use, distribution and reproduction in any medium, provided the original work is properly cited.

© 2025 The Author(s). Macromolecular Materials and Engineering published by Wiley-VCH GmbH

and alkaline dust and negatively impacting air quality. RM disposal also requires large land areas, with $\approx 1\text{--}1.5$ tons of RM being generated per ton of alumina, and the demand for alumina continually increasing worldwide [11]. Based on current forecasts, an accumulation of up to 8 billion tons of RM worldwide is expected by the year 2040, increasing waste management strategy concerns [12].

The composition of RM is complex and varies depending on the geographic origin of the ore as well as the specific process conditions in the Bayer process. On average, it mainly consists of Fe_2O_3 (5–60 wt.%), Al_2O_3 (5–30 wt.%), TiO_2 (0.3–15 wt.%), CaO (2–14 wt.%), SiO_2 (3–50 wt.%) and NaO (1–10 wt.%) with also trace amounts of rare earth elements (REE), e.g., Sc, Y, Nd, Dy, and V (≈ 0.1 wt.%) [7, 9, 13, 14]. Efforts have been made to utilize RM either as a feedstock or as a source of raw materials to reduce waste deposits and to explore its commercial valorization. Currently, RM has been proposed for use in the construction industry as a bulk raw material, specifically as a filler in asphalt and building materials such as concrete and bricks, including thermally and impermeable materials [11, 15–19]. On a smaller scale, RM can also be utilized as a source of valuable metals through various hydrometallurgical treatments for semi-selective recovery of Fe, Al, Ti, and critical REEs, from which the final effluent remains as a solution containing the leaching acid and minor concentrations of various metals [16, 20–26].

At the same time, 10.5 million tons of starch—used in the food, biofuel, and paper industries—were produced in 2022, generating ≈ 5 million tonnes of proteins and fibers as by-products [27]. As the demand for bioethanol continues to rise as an attractive alternative to fossil fuels [28], an excess of proteins is continuously produced. Proteins are natural polymers, and by combining different proteins, synergistic effects can be harnessed to produce thermoformed materials with various functionalities, such as extruded biofoams for the replacement of fossil-based single-use plastics [29–36].

Single-use polymeric foam materials have a range of important industrial applications thanks to affordability, low density, and thermal resistance, where they provide various functionalities such as absorption capacity, impact resistance, thermal-, electrical-, and sound insulation. Current commercial single-use polymeric foams consist mainly of fossil-based, hence carrying the associated issues of high greenhouse gas emissions and slow degradation in natural environments, where they instead contribute to the widespread distribution of microplastics [32, 37]. Therefore, there exists a need to find sustainable alternatives to our traditional synthetic polymers in all their current and potential future application areas [38]. In this context, wheat gluten (WG) and zein (Z), from wheat and corn production, respectively, represent a good alternative. Using natural polymers such as gluten and zein in foam materials would reduce the negative environmental impacts of synthetic polymers while the cohesive and viscoelastic properties of gluten and the overall processing versatility of zein allow foam production via conventional plastic manufacturing methods such as extrusion [29, 32, 37, 38]. Likewise, metal ions can be used to engineer these protein foams, granting them different thermodynamic stability and favoring folding/unfolding equilibrium by mediating crosslinks between proteins [39]. Different metals can provide characteristics to

TABLE 1 | Main components of red mud and their respective concentrations.

	Fe	Al	Si	Ca	Ti
RM (wt.%)	208	108	57	36	25
	Ce	La	Sc	V	Y
RM (ppm)	355.5	166.7	96.0	378.4	97.9

the polymeric chains and, consequently, to the foams, rigidity, hardness, and elasticity [40]. Thus, with large-scale applications of red mud being desirable, utilizing it as a secondary source for metal ions may be of interest in the context of trying to improve the mechanical properties of extruded protein-based foams. However, work remains to be done regarding optimizing the porous network for different applications as well as achieving good mechanical stability of the foams.

In this work, we address the dual challenges of replacing single-use, fossil-based polymeric foams with bio-based alternatives and upcycling red mud. By utilizing red mud instead of a single metal, the additive becomes a complex mixture of metals, either as metal oxides in the raw red mud or as a metal solution in the oxalic acid leachate. This approach allows for various possibilities of metal-protein interaction, increasing the likelihood of crosslinking and other effects, and potentially developing diverse properties in the final extruded material. The goal is to develop foams using blends of wheat gluten and zein and to investigate the impacts of incorporating red mud (either as leachate or raw red mud) on the physical and mechanical properties of the product through the characterization of the extrudates. The developed formulations were analyzed regarding morphology, density, swelling capacity, and mechanical properties.

2 | Experimental Section

2.1 | Material

The wheat gluten powder was supplied by Lantmännen Reppe AB, Sweden (86 wt.% protein content) as a co-product from industrial wheat starch production. Zein protein from corn was purchased from Sigma–Aldrich, Sweden (88–96 wt.% protein content). Glycerol (99%), sodium bicarbonate (NaHCO_3 , > 99.7%), and Oxalic Acid were purchased from Fisher Scientific (Sweden) and Sigma–Aldrich (Sweden), respectively. The raw red mud was provided by ETI Aluminum (Turkey). The main components and their concentrations are shown in Table 1.

2.2 | Red Mud Leaching

Raw red mud was leached with 1 N oxalic acid in a liquid–solid ratio of 50:1 for 24 h under constant stirring at room temperature. The final suspension was filtered, and the resulting solution, referred to as oxalic acid leachate (HOx), was directly used in the formulations. The metal composition of the leachate was determined using Inductively Coupled Plasma Optical Emission Spectroscopy (ICP-OES, iCAP 7000 Series, Thermo Scientific).

TABLE 2 | Compositions of the extrudates in the RM-experimental design, with the corresponding normalized values in parentheses.

Sample	MQ	Gly	SBC	RM
75Z	5	50	0 (−1)	0 (−1)
75Z/SBC			5 (+1)	0 (−1)
75Z/RM			0 (−1)	5 (+1)
75Z/SBC/RM			5 (+1)	5 (+1)
75WG			0 (−1)	0 (−1)
75WG/SBC			5 (+1)	0 (−1)
75WG/RM			0 (−1)	5 (+1)
75WG/SBC/RM			5 (+1)	5 (+1)

2.3 | Extrudates Formulation

The prepared mixtures were based on wheat gluten (WG), zein (Z), glycerol (Gly), sodium bicarbonate (SBC), and MilliQ-water (MQ), with and without the addition of leachates or raw red mud as powder. The content of Gly (50 wt.%), SBC (5 wt.%), and MQ (5 wt.%) was based on previous studies [35], where good extrudability was obtained. The leachate solution and RM powder were each added at 5 wt.% based on the total protein content (preliminary experiments with higher concentrations yielded no expansion for 50 wt.% RM and clogging of the extruder for 50 wt.% HOx). Before using the RM as an additive, it was coarsely grounded in a mortar to break up agglomerates and then heated in an oven at 100°C for 24 h to remove adsorbed water. After drying, it was ground again into a fine powder.

A full factorial design with 3 factors, each at 2 levels, was conducted for the samples extruded with raw red mud powder (RM). The three varied parameters were the WG:Z ratio, and the presence or absence of SBC and RM. The eight experimental conditions (2^3) are presented in Table 2. The WG:Z ratio is shown in the first column. For simplicity, the label included only the component in higher proportion, 75 wt.% (the other component is always at 25 wt.%). The label also includes information on the addition of SBC and RM, which were varied at 0 and 5 wt.%. The table also includes the values for 0 and 5 wt.% respectively, as low (−1) and high level (+1) in the design matrix.

A two-level full factorial design (2^2) was used as a basis for the number and composition of different samples to be extruded. The presence or absence of two components in the formulations was investigated for significant effects on the extrudate's properties: HOx and SBC. Table 3 presents the composition values of each of the four samples extruded in the HOx-experimental design. The labeling follows the same reasoning as Table 2.

2.4 | Extrusion

A micro-compounder co-rotating double-screw DSM Xplore 5 (the Netherlands) with a circular die of 3 mm in diameter was used for extruding the formulation mixtures. The temperature in all three sections of the extruder was set to 100°C and the extrusion speed to 60 rpm, based on previously established

TABLE 3 | Compositions of the extrudates in the HOx-experimental design, with the corresponding normalized values in parentheses. The weight percentages are relative to the total protein content.

Sample	MQ	Gly	SBC	HOx
75Z	5	50	0 (−1)	0 (−1)
75Z/SBC			5 (+1)	0 (−1)
75Z/HOx			0 (−1)	5 (+1)
75Z/SBC/HOx			5 (+1)	5 (+1)

optimal values [35]. The extrudates were kept in a desiccator over silica gel for 1 week before analysis.

2.5 | Characterization

2.5.1 | Rheology

The mixtures first had to be compressed into thin discs with a diameter approximately matching that of the rheometer probe (25 mm) to test the rheological properties of and establish processing windows for the formulation mixtures. This was done using a hot press set at a temperature of 20°C and applying a force of 100 kN for 2 min. A metal template plate of 1 mm thickness with 24 (3 × 8) cut-out circles of ≈25 mm in diameter was used to get appropriate disc sizes. Triplicate specimens were compressed for each formulation mixture.

Rheological measurements were carried out in a Discovery HR-2 Hybrid Rheometer (TA Instruments, USA) in shear mode, using a parallel plate geometry (parallel plate of 25 mm and a Peltier plate to achieve the set temperature). First, strain sweep tests were performed to determine the linear viscoelastic range (where the storage- and loss- moduli curves are constant and independent of the applied strain). For these tests, the temperature and frequency were fixed at 20°C and 1.0 Hz, respectively, while the strain was set to range from 0.002% to 2%. Subsequently, frequency sweep tests were carried out at a constant strain and temperature of 1% (within the linear viscoelastic range) and 20°C, respectively, with the frequency ranging from 0.2 to 20 Hz. Finally, temperature ramps were performed from 20 to 150°C, with constant strain- and frequency values determined from the two previous sweeps (0.01% and 1.0 Hz). The heating rate was set to 10°C/min. Values of the elastic- (storage modulus) and viscous (loss modulus) moduli were collected (G' and G'' respectively) as well as the damping factor $\tan(\delta)$ ($= G''/G'$). Measurements were performed in duplicate.

2.5.2 | Apparent Density

The apparent densities of the dry extrudates were estimated in triplicate for each sample. A caliper was used for diameter and length measurements, and a scale (Mettler Toledo AL104) was used for weighing the specimens. The density was then estimated by dividing the mass of each specimen by its volume, assuming a cylindrical shape, and reporting the apparent density of the sample as an average of triplicates with standard deviations.

2.5.3 | Liquid Swelling Capacity

The 'tea bag test', according to the nonwoven standard procedure (NWSF) 240.0.R2, was used to estimate the free swelling capacity (FSC) of the dry extrudates. For each extrudate, specimens with a weight of ≈ 200 mg were each put in a dry, non-woven tea bag, hooked on a rod, and immersed in MQ-water for 1, 5, 10, and 30 min. After each immersion time, the bags with the specimens were hung for 10 s outside of the liquid. One by one, they were then placed on tissue paper for 10 s to remove excess water and thereafter weighed. The swelling capacity for each extrudate is reported as an average of triplicates with standard deviations using Equation (1):

$$FSC \text{ (g/g)} = \frac{W_i - (CF \cdot W_b) - W_s}{W_s} \quad (1)$$

where W_i is the weight of the bag and sample after immersion, CF is the correction factor (estimated from the average swelling of three empty bags), W_b is the weight of the empty dry bag, and W_s is the weight of the dry extruded specimen.

2.5.4 | Mechanical Properties

After having kept the extrudates for conditioning at $21 \pm 0.14^\circ\text{C}$ and $50\% \pm 0.47\%$ RH for 48 h, static tensile tests were performed in a Universal Testing Machine (single column, Instron 5944) with a 500 N load cell. For each extrudate, five specimens were measured. The strain rate used was 10%/min. From the stress-strain curves generated, values for Young's modulus, yield strength, ultimate tensile strength, and strain (extension) at maximum stress could then be obtained as an average with standard deviations.

2.5.5 | Microstructure

Extrudate morphologies were investigated under SEM (Hitachi Tabletop SEM TM-1000 at 10 kV acceleration voltage). Sample preparation was carried out by immersing the specimen in liquid nitrogen and thereafter shattering it to expose the cross-section surface area.

2.5.6 | Protein Structure

Effects of the extrusion and metal incorporation on the protein secondary structure were studied using a PerkinElmer UATR Spectrum, two FT-IR spectrometers connected to the PerkinElmer IR software, version 10.6.2. Spectra were gathered in a range of 600–4000 cm^{-1} , with 16 consecutive scans (accumulations) per sample. Before analysis, the extrudates were dried in a desiccator over silica gel for at least 1 week to minimize the interferences of water.

2.5.7 | SDS Protein Extractability (Estimation of Crosslinking Degree)

1 g of each extrudate material was submerged in 1 mL of 0.1% (w/v) sodium dodecyl sulfate (SDS) solution and stirred at 37°C

at 1500 rpm for 30 min. The mixtures were centrifuged at 8000 g for 5 min at RT, and the resulting supernatants were mixed with 4 \times SDS-PAGE loading buffer. Samples were denatured by heating at 95°C for 5 min and analyzed by SDS-PAGE. The electrophoresis was conducted for 25 min at 150 V by loading 15 μL of each sample per well into Mini-PROTEAN TGX Stain-Free Precast Gel (Bio-Rad). 5 μL of Precision Plus Protein Unstained (Bio-Rad) was used as molecular weight ladder. The gel images were captured using a Chemidoc MP imager (Bio-Rad).

3 | Results and Discussion

The analysis of HOx (Section SI, Supporting Information) showed that the main components (Fe, Al, Si, Ca, and Ti) were leached in higher proportions without much selectivity. Minor concentrations of cerium and yttrium were also measured.

3.1 | Extrusion

Figure 1a,b,e,f shows the appearance, composition, and expansion ratios (ERs) for the four reference extrudates without HOx or RM. Comparing the colors between the samples, the ones without SBC can be seen to be dark brown, while the foams with SBC appear light yellow. The browning of the non-SBC samples, compared to the bright yellow color of the 75Z protein blend mixture during extrusion, is indicative of reactions occurring that involve the amino acid residues of the proteins, e.g., Maillard reactions (i.e., non-enzymatic browning reaction of reducing sugars with amino acids) [41].

The expansion ratios (ERs) of the samples were in the range of 1.04–1.36 \pm 0.1. As expected, the extrudates containing SBC had significantly higher ER values compared to corresponding non-SBC samples. The ER for the 75Z extrudate increased by around 30% upon the addition of SBC. Yet, the 75Z extrudates were brittle and hard in texture, easily snapping upon bending. These directly apparent behaviors were expected due to the lower glass transition temperature (T_g) of zein, in higher proportion in this formulation, compared to wheat gluten, turning the extrudates glassy and hard at room temperature, as opposed to viscoelastic properties of gluten (which would turn the extrudates soft and flexible).

The appearance, composition, and corresponding ER-value of two samples extruded with 5 wt.% HOx can be seen in Figure S1. The colors of the 75Z/5HOx samples (without and with SBC) can be seen to be comparable to the corresponding reference extrudates without HOx (Figure 1e). However, the ER values are higher. For both samples, with and without SBC, the ERs are 1.45 and 1.54, respectively, which are 38 and 12% higher than the extrudates without HOx. The difference in ER between the HOx samples with and without SBC (6%) is barely significant compared to the difference between the corresponding reference samples. The increased ER values observed for the HOx-containing extrudates independently of the SBC may indicate increased crosslinking during the extrusion process. The T_g would be expected to increase due to the formation of a more rigid protein network with restricted inter-chain mobility, while increased crosslinking would also have an effect in reducing pore size via network

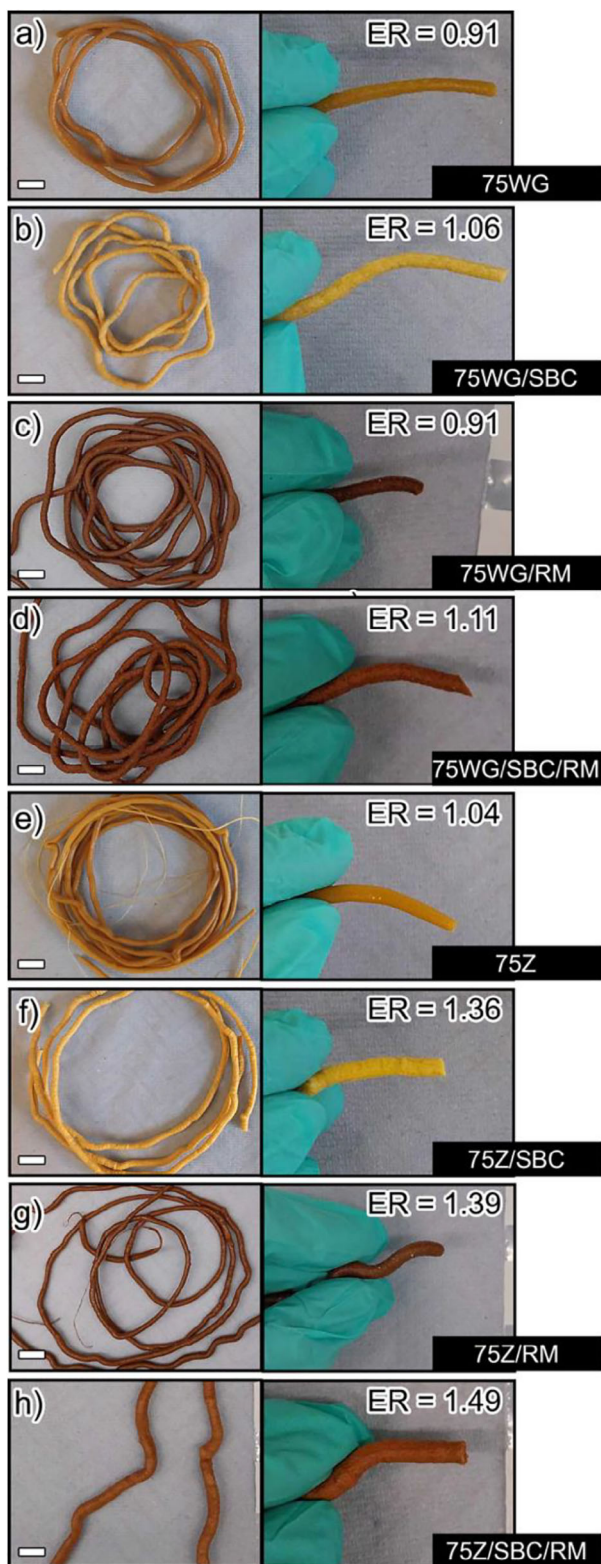


FIGURE 1 | Macroscopic images of the extrudates with corresponding expansion ratios (ER) of the blends (a) 75WG, (b) 75WG/SBC, (c) 75WG/RM, (d) 75WG/SBC/RM, (e) 75Z, (f) 75Z/SBC, (g) 75Z/RM, (h) 75Z/SBC/RM.

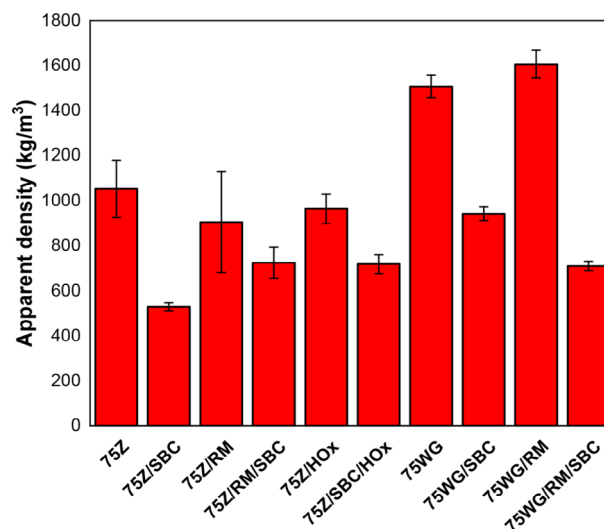


FIGURE 2 | Estimated apparent densities of extrudates.

collapse once foaming agent pressure is reduced, leading to lower ER [34]. Water has previously been shown to promote the collapse of medium-sized pores [35], explaining lower ERs in formulations without HOx.

Figure 1c,d,g,h presents images of each sample extruded with 5 wt.% RM added to the formulations with 75WG and 75Z. The colors of the filaments appeared darker brown after extrusion compared to the light brown/red formulation mixtures pre-extrusion, thus following the same trend of shifting from lighter to darker color shades during extrusion as observed for the reference and HOx samples. Again, samples containing SBC exhibited a lighter shade of color and higher ER values compared to samples without SBC (see Figure 1d,h). The RM extrudates based on the 75Z protein blend displayed higher ER compared to the corresponding reference samples. The 75Z/RM samples without and with SBC had ERs 34 and 10% higher than the reference, respectively. Lower ERs were obtained for the samples based on the 75WG blend compared to the 75Z blend. Significant increases in ER values were obtained for the 75Z/RM, 75Z/SBC/RM, and 75WG/SBC/RM extrudates.

It is noteworthy that there are limitations to the extrusion of formulations based on a 75WG protein blend. The higher content of WG entails different viscoelastic properties, yielding higher surface roughness and pressure increase during extrusion, which can lead to clogging of the equipment. The blends with higher zein content yielded smoother surfaces, thus avoiding machinery issues. The effect of extruding porous protein-based materials with high gluten content has already been reported elsewhere [35].

3.2 | Physicochemical and Absorption Properties of the Extrudates

The estimated apparent densities of the extrudates are shown in Figure 2. The values range from 500 to 1600 kg/m³, with the lowest- and highest densities associated with the 75Z/SBC reference sample and the 75WG/RM extrudate, respectively.

Categorizing the samples into low (<800 kg/m³), medium (800–1000 kg/m³), and high (>1000 kg/m³) density foams, the following trends are apparent: the SBC-containing foams generally have the lowest densities; foams high in WG have higher densities compared to foams with a higher Z content; and the maximum density is associated with the sample high in gluten and containing RM. These trends are expected. Since SBC is a foaming agent, it leads to high porosity, hence increasing the 'empty' volume within the extrudate. At the same time, gluten has a higher molecular weight than zein, and RM is a heavy additive due to its high metal content.

Adding HOx to the 75Z blend results in a slightly lower density in the blend without SBC (−7%) while increasing the density of the foam with SBC (+36%). The difference in density between the HOx samples without and with SBC compared to the corresponding references is smaller, which may indicate that HOx and SBC interact to lower the effect of SBC. This corroborates the smaller difference in expansion ratio between porous and non-porous samples containing HOx.

RM increases the density of the 75WG/RM (+7%) as well as the 75Z/SBC/RM sample (+37%) while lowering the density of the 75WG/SBC/RM (−25%). As for the RM containing 75Z foams, the density difference is smaller between the non-porous and porous samples as compared to the references, which is also correlated with the smaller difference in expansion ratio between the porous and non-porous 75Z samples containing RM. As for the 75WG samples with RM, the difference in density between the non-porous and porous samples is considerably larger, and the difference in ER between the same samples was also larger compared to the references. This hints at the development of a porous network with relatively large pores.

Figure 3a–c shows the SEM images obtained for the extrudate cross sections and surface. For all samples, the porosity can be seen to be higher when SBC is present (Figure 3a–c), which agrees with the apparent density results (Figure 2), i.e., higher density correlating to lower porosity. Looking at the reference foams containing SBC, the 75WG system (Figure 3a) seems to have a relatively wide pore shape and size distribution, while the 75Z system (Figure 3c) appears to have relatively high porosity and regular pore shapes and sizes. No porosity is apparent in the reference foams without SBC or on the surface of the samples (Figure 3a,b). However, for the 75Z samples with RM and HOx (Figure 3c and Figure S2, respectively), closed-cell pores can be seen to have developed without the presence of SBC. Some pores are expected due to the presence of water, with mainly small closed-cell pores having been reported previously for foams with a high WG content without SBC [32, 35]. The higher porosity is apparent in Figure 3 for the foams without SBC and with HOx and RM compared to the references matches the relatively low apparent densities of these foams.

The 75Z/SBC samples with HOx and RM exhibit mainly closed-cell porosity with relatively regular pore shapes. It can be observed that the 75Z/SBC/RM sample (Figure 3c) shows relatively high porosity with large pore sizes compared to the 75Z/SBC/HOx (Figure S2). The 75WG/SBC/RM (Figure 3a) exhibited more open-cell porosity with larger- and more interconnected pores compared to the reference sample (i.e., 75WG and

75WG/SBC), which is consistent with the lower apparent density estimated for this sample relative to the reference. Clusters of metals can be seen both in the 75Z/RM and 75WG/RM (Figure 3a–c, respectively, and Figure S3).

In a previous study by Hurtado et al. [34] no major difference in microstructure could be observed between samples crosslinked with 2.5 wt.% of the natural crosslinking agent genipin as compared to controls. However, a slight decrease in pore size was obtained for the crosslinked samples. This was related to the microstructure of a more crosslinked material, which is characterized by smaller or absence of pores due to the development of a more elastic porous network that collapses once the pressure generated by the foaming agent is reduced. Based on the microstructures of the foams containing HOx and RM, an increase in crosslinking density is still unclear.

The average swelling capacities (FSC) are presented in Figure 4 for non-SBC (Figure 4a) and SBC containing extrudates (Figure 4b). The value ranges match results obtained for similar samples as reported in the literature [35]. Generally, dips between data points can be observed that cause a zig-zag pattern of the curves. The decrease in FSC in between weighing is due to the mass loss of glycerol, which is highly soluble in water [32, 25]. The zig-zag pattern can thus be observed for the curves corresponding to the samples where more mass is lost via glycerol diffusing into the water than mass gained by water absorption.

The highest FSC was obtained for the 75WG/RM formulation, both without (≈2.5 g/g) and with (≈4.0 g/g) SBC, while the 75WG reference sample had the lowest FSC overall (≈1.5 g/g). Thus, RM seems to increase swelling for foams with a higher gluten content. A higher FSC was also obtained for the 75WG/SBC/RM, which points to a foam network structure with open-cell porosity. This is consistent with the low density estimated for this sample as well as the relatively large pore size observed in SEM.

Based on the overall results, HOx cannot be said to change the swelling capacity of the 75Z blends significantly. This could be related to the development of a network characterized by more closed-cell porosity and smaller pores, as has been reported by Bettelli et al. [32] when carboxylic acids are used as additives. However, adding RM has increased the swelling capacity of the 75WG samples (without and with SBC), with the largest increase obtained for the foam containing SBC.

Figure 5a–e shows the rheometric analysis for each sample formulation mixture, with the storage modulus (G'), loss modulus (G''), and $\tan(\delta)$ ($=G''/G'$) plotted against temperature. As a general trend, both moduli decrease until an inflection point, after which they stabilize at lower values relative to the initial plateau values. Thus, the plots can be divided into three distinct regions where the mixtures exhibit different flow properties. The first region is known as the glassy area and occurs at temperatures below T_g [42]. This area is characterized by the highest moduli values, as the protein chains are locked in fixed positions with low chain mobility. The G' values are high since relatively large forces are required to change the polymer conformations. This region is only present in the 75Z samples

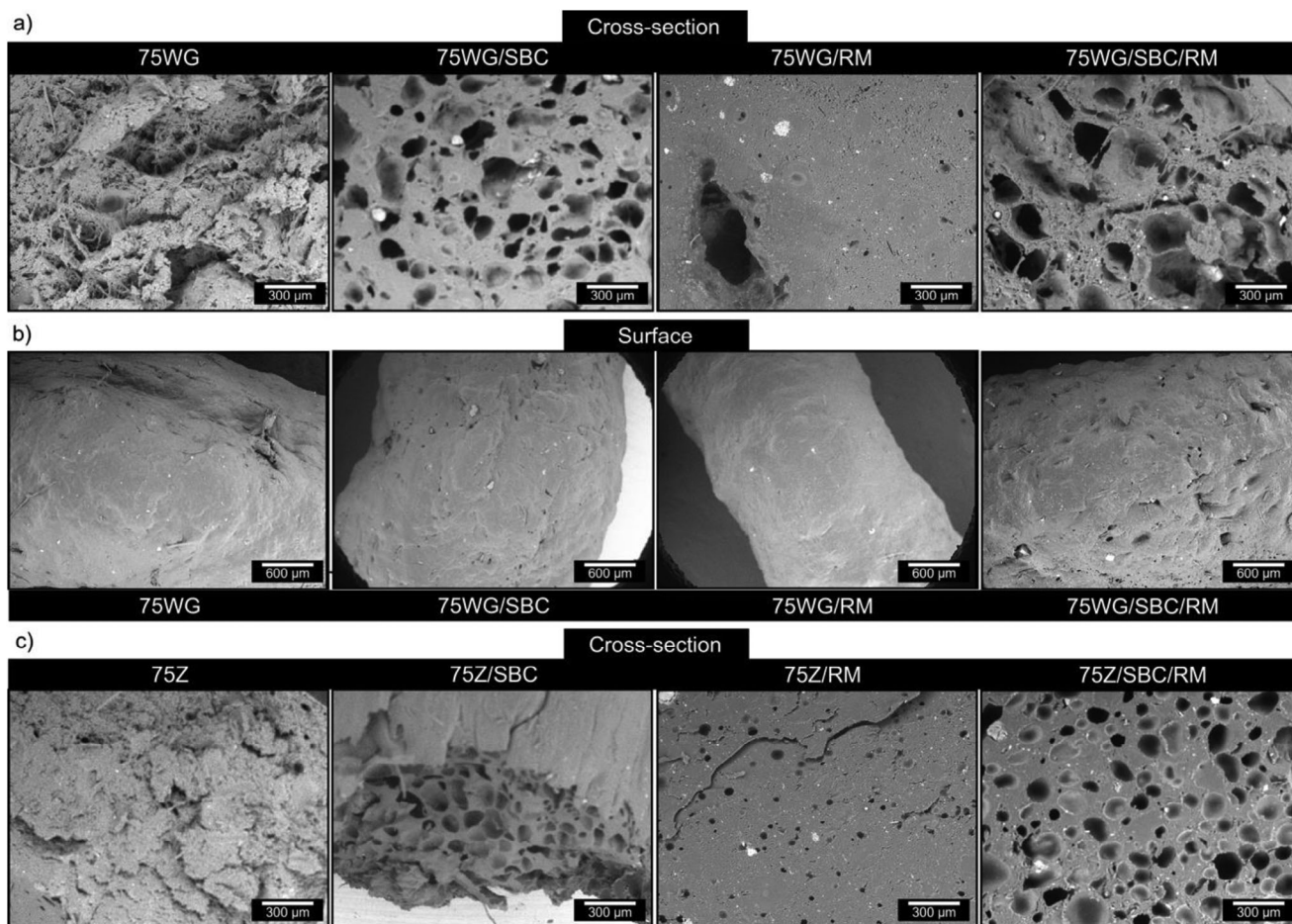


FIGURE 3 | SEM images of extrudate cross-sections and 75WG systems surface.

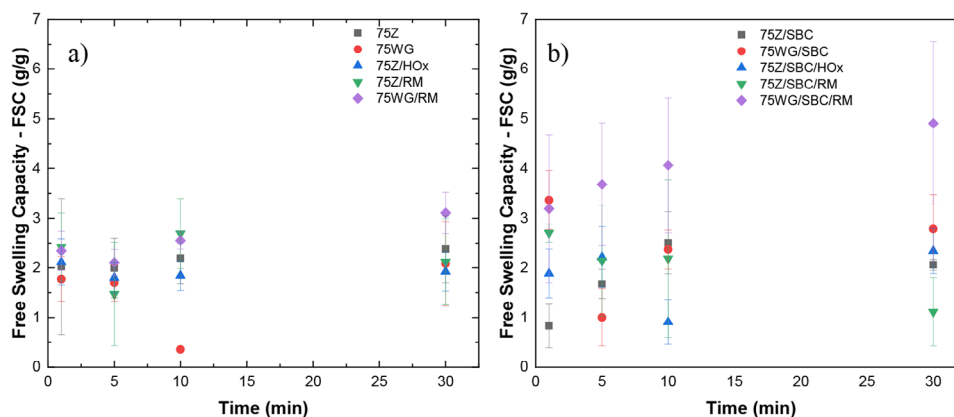


FIGURE 4 | Free liquid swelling capacity [g/g] for extrudates (a) without SBC and (b) with SBC in MQ-water.

(20–70°C), demonstrating the higher structural stability of this protein. As temperature increases, the thermal energy starts to break up crosslinks between protein chains, which increases chain mobility. The second region, the glass transition region (70–140°C for 75Z samples and 20–120 for 75WG ones), is where segments of the polymer chains can start to move freely. The temperature at the inflection point of the curve is the T_g , where the polymer goes from being hard and glassy to soft and flexible. This transition causes the modulus to decrease rapidly, and the

polymer becomes like leather in texture [43]. After the glass transition region comes the rubber plateau zone, where the chain segments are relatively mobile, and the polymer appears softer and more flexible compared to the case in the transition region. The chains are still held together via entanglements, and the modulus barely changes with increasing temperature in this region until the viscous zone is reached and the modulus drops as chain entanglements are broken, and the chains can irreversibly drift apart to yield a fluid state [44].

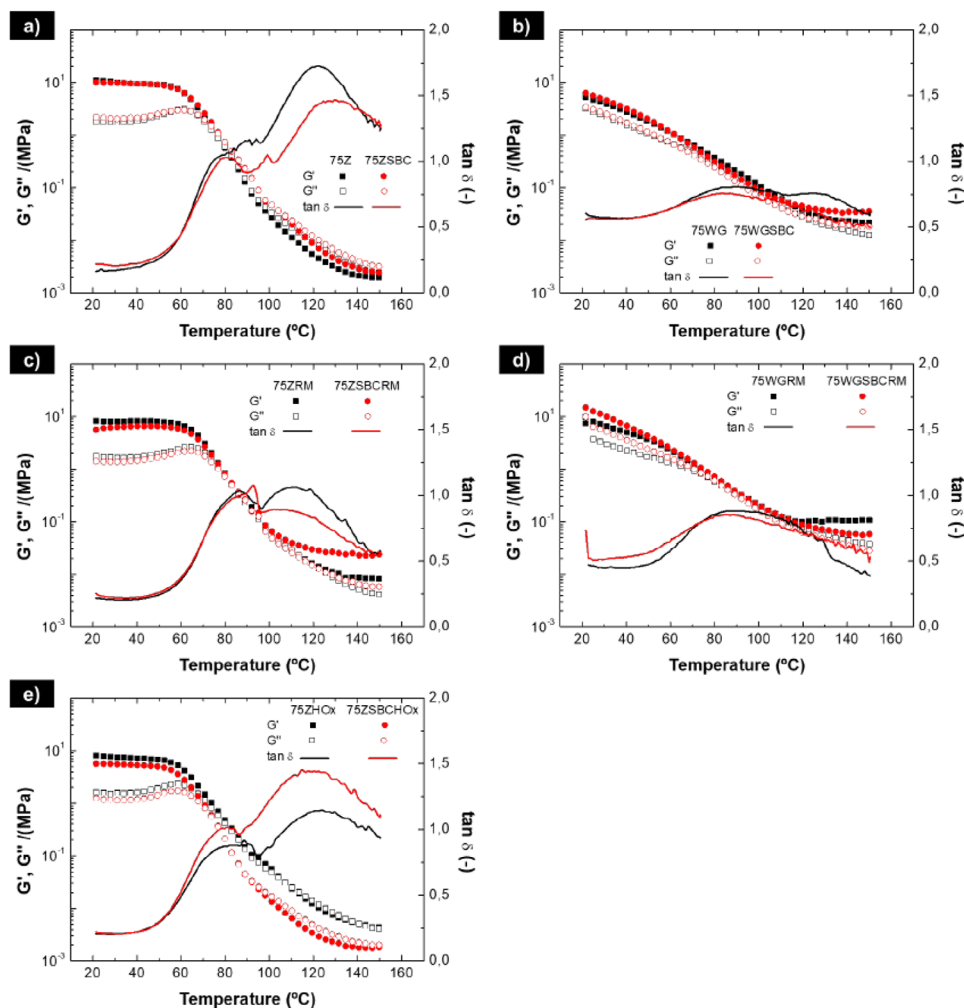


FIGURE 5 | Temperature ramps from rheometric analysis of the formulation mixtures pre-extrusion: (a) 75Z and 75Z/SBC, (b) 75WG and 75WG/SBC, (c) 75Z/RM and 75Z/SBC/RM, (d) 75WG/RM and 75WG/SBC/RM and (e) 75Z/HOx and 75Z/SBC/HOx. All mixtures contain 5 wt.% MQ and 50 wt.% glycerol (relative to the total protein content).

The T_g of the proteins corresponds to the inflection point of the G' -curve as well as the maximum value for $\tan \delta$ in the glass transition region [45]. The average T_g values were determined from the $\tan \delta$ curve for each formulation mixture (Table S2). The values span from 80 to 100°C. According to the estimated T_g values, adding HOx or RM to the formulation mixtures does not result in significant changes in T_g . The $\tan \delta$ values can be seen to be higher for the reference blends with a higher zein content compared to the blends with a higher gluten content. The higher values for the zein blends are consistent with the higher viscosity of zein compared to gluten, yielding a larger loss modulus (G'') relative to the storage modulus (G'). The opposite case holds for gluten, with lower $\tan \delta$ values due to its higher elasticity (G') relative to viscosity (G'') [35].

Generally, lower T_g values were obtained for the mixtures containing SBC, although they do not show significant differences. A less steep decrease in the moduli values in the inflection zone is expected for the samples with SBC, resulting in higher values after transition. The effect has been attributed to the greater porosity of the SBC samples, which potentially alleviates the decrease in moduli at higher temperatures [35]. This can be observed for

all mixtures except for the 75WG/RM formulations (Figure 5d), where higher moduli values are seen after the inflection point for the mixtures without SBC.

Additionally, the G' - and G'' -curves do not drift apart from each other after the glass transition through a large temperature interval as the reference. Since closer proximity of the moduli values corresponds to higher flow and deformability [35], the rheological behavior does not seem to change as much at temperatures above 100°C compared to the glass transition region. Again, this could be due to a plasticizer effect induced by the presence of oxalic acid that enhances the viscosity of the 75Z formulation [46].

Adding RM to the 75Z (Figure 5c) resulted in a less steep decrease in G' values relative to G'' values, with the storage modulus values considerably larger than the loss modulus after glass transition ($\tan \delta < 1$). Thus, both mixtures exhibited a more elastic than viscous character at higher temperatures (after glass transition) compared to both the reference and the mixtures with HOx. This behavior could be related to the increase of elasticity via protein crosslinking with the RM metals after the glass transition. The

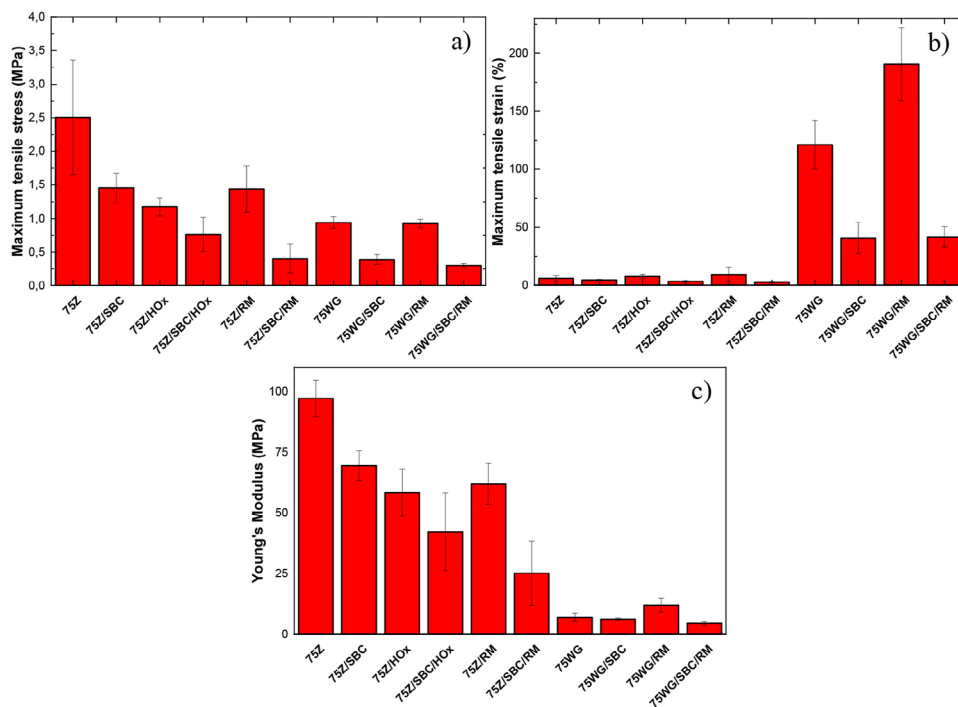


FIGURE 6 | (a) Maximum tensile stress [MPa], (b) maximum tensile strain [%], and (c) Young's modulus [MPa] for each extrudate.

transition region can also be seen to be broader for the RM blend without SBC, with the G' and G'' curves following each other closely up to $\approx 120^\circ\text{C}$. This indicates a larger processing window compared to the reference, which is relevant for future industrial applications where broad processing windows are preferable.

In the realm of works related to the extrusion of similar porous materials, such as polyurethane (PUR) and starch-based foams, processing typically occurs at foaming temperatures $\approx 180^\circ\text{C}$ and rotational speeds of 100 rpm. The results in this study suggest that, even with the incorporation of inorganic additives such as red mud, our extrusion process operates at lower temperatures than those commonly reported for PUR. This highlights the potential for energy-efficient processing, and future works should explore how energy and material output compare with those of relevant bio-based materials [47, 48].

In the 75WG/RM blends, an increase is observed in initial values of G' and a less pronounced decrease in storage modulus values over the whole temperature range as compared to the reference mixtures (Figure 5b–d). The loss modulus values also decreased less rapidly and stabilized at a higher level. This indicates that RM increases the solid character of the 75WG mixtures. The increase in solid character could be due to the RM promoting crosslinking. In terms of the difference between the G' and G'' curves, the glass transition region is easier to observe compared to the references due to the closer proximity of the moduli curves in that temperature range. This indicates that RM increases the viscous character of the 75WG mixtures during glass transition.

Figure S4 shows representative stress–strain curves for each sample tested, while Figure 6 presents the average values with standard deviations for the maximum stress (σ_{\max}), strain (ϵ_{\max}), and Young's modulus. It is noteworthy that, despite efforts to

uniformly extrude the materials, inherent irregularities such as scratches, pits, and some variation in the cross-sectional areas throughout the material may cause the relatively large standard deviation seen in the results for the mechanical properties. Harder and glassier samples are expected to show higher stress and lower strain at break (high ϵ) in contrast to more soft and elastic foams that should exhibit higher strain values (lower ϵ). Additionally, the more brittle the sample, the lower the strain it can handle before fracturing. The results are consistent with these expectations: foams based on the 75Z protein blend (hard and glassy in texture) exhibited lower strain (Figure 6b) and higher Young's modulus values (Figure 6c) compared to the samples based on the 75WG blend (soft and flexible in texture). The more brittle SBC foams all had lower stress, strain, and ϵ values compared to the corresponding samples without SBC.

The highest average maximum stress (2.5 MPa) and Young's modulus (97 MPa) were obtained for the 75Z reference sample, while the minimum average stress (0.3 MPa) and Young's modulus (4.6 MPa) were obtained for the 75WG/SBC/RM sample. The low values of the RM-containing foam may correlate to its relatively low density and high swelling capacity compared to the reference (75WG/SBC). In terms of average strain, the maximum value (190%) was obtained for the 75WG/RM foam, while the 75Z/SBC/RM sample had the minimum strain (2.7%). Overall, the SBC containing extrudates had lower maximum stress-, strain-, and Young's modulus compared to their non-SBC counterparts. This is expected since the SBC samples have higher porosity, with pores acting as defects in the material and making it more vulnerable to the formation of cracks and, thereby, breakage. The maximum stress at break is in accordance to previous works on protein-based porous materials showing circa 2–2.5 MPa [34, 49]. However, Young's modulus and maximum strain in this work are respectively ≈ 200 and 6 times higher, demonstrating the impact

of RM in plasticizing the material without significant losses of extensibility, corroborating with the rheology results.

Adding HOx to the 75Z blend decreased stress and Young's modulus, while the strain remained almost unaltered. Exchanging HOx with RM in the same blends had no significant impacts. Adding RM to the 75WG blends lowered tensile stress for the SBC sample, while the sample without SBC exhibited a significant increase in strain and no major changes in stress and Young's modulus.

An increase in crosslinking density is expected to yield foams with increased stress and decrease strain due to the formation of a more dense and rigid protein network with less mobility between protein chains [34]. Thus, the addition of HOx or RM to the blends does not result in the typical mechanical behavior in the presence of commercial crosslinking agents. The results indicate that HOx and RM as additives yield a less dense and rigid protein network with increased mobility between chains. This is consistent with the results obtained from the rheological measurements that suggested HOx acts as a plasticizer to increase chain mobility. In the case of both RM and HOx, the more plastic behavior could also be accounted for by longer crosslink bridges forming. This may especially apply to RM, which induced greater increases in sample strain. A strain-increasing effect has been reported previously by Hurtado et al. [34] when genipap oil was used as an additive and compared to commercial genipin as a crosslinking agent. The effect was hypothesized to occur due to additional components in the genipap oil acting as formulation plasticizers and/or the development of longer crosslinks between protein chains.

Since both the HOx leachate and the RM powder are multicomponent additives, they are potentially contributing to several effects simultaneously. Added in the form of oxalic acid leachate, the metals in red mud are present in an acidic aqueous solution, chelated by the conjugate bases of oxalic acid (hydrogen oxalate HC_2O_4^- and oxalate $\text{C}_2\text{O}_4^{2-}$). Using red mud as a dry powder eliminates some components while introducing others, thereby it is more alkaline than acidic, and the metals are mostly present as oxides in a different composition compared to the leachate. The results presented here thus reflect the combined effects of all these components. Future work should study the effect of the different components forming RM (blends of oxides and minerals) on the protein blends individually, which can allow to differentiate the specific role of each component more systematically.

Normal probability plots for the maximum tensile stress and strain results for the HOx and RM experimental designs are shown in Figure 7a–d, respectively. For the HOx experimental design, with two main parameters (HOx and SBC content) and one interaction parameter, all three parameters influence the maximum tensile stress according to Figure 7a. Extruding the mixtures with either HOx or SBC significantly decreases tensile stress (negative effects), while adding both increases the stress via interaction effects (positive effect). These results match the trends observed in Figure 6a. The negative effect of adding either SBC or HOx corresponds to the 75Z/SBC samples exhibiting lower stress compared to the ones without SBC and to HOx lowering stress in the blend without SBC. The positive interaction effect would mean that the stress for the HOx system with

SBC does not decrease as much as would be expected based on the stress difference between the reference samples, with HOx possibly lowering the stress-reducing effects of SBC. The effects of the parameters on the maximum tensile strain appear to be insignificant, according to Figure 7b.

For the RM experimental design, with three main parameters (WG:Z ratio, SBC content, and RM content) and four interaction parameters, the tensile stress seems to be significantly impacted by three of the factors. According to Figure 7c, the SBC content has a negative effect; there is a negative interaction effect between the WG:Z ratio, SBC, and RM, as well as a positive interaction effect between the WG:Z ratio and the RM. The negative effect of SBC would translate to lower stress for samples with SBC compared to those without, which has already been established according to Figure 7a. The negative interaction effect between WG:Z ratio, SBC, and RM corresponds to the result showing the high gluten content blend with SBC and RM to exhibit the minimum stress (Figure 6a). Lastly, the positive interaction between the WG:Z ratio and the RM would result in a smaller difference than expected between the 75Z/RM and 75WG/RM samples compared to the references, indicating that the RM acts to lower the stress-reducing effect of a high gluten content—also seen in Figure 6a.

Four parameters are deemed significant with respect to their effect on strain in the RM experimental design, as evidenced by Figure 7d: WG:Z ratio (positive effect), SBC (negative effect), the interaction between SBC and RM (negative effect), and the interactions between WG:Z ratio and RM (positive effect). A positive effect for the WG:Z ratio corresponds to the higher strain values observed for the 75WG compared to the 75Z formulations (Figure 6b). The negative interaction between SBC and RM is also supported by Figure 6b, where lower strain values than the references were obtained when RM is added to formulations with SBC. Finally, the positive interaction between the WG:Z ratio and RM also matches the observations that strain values increase between the 75Z and the 75WG blends when RM is added, meaning that the RM further reinforces the strain-increasing effect associated with a higher gluten content blend.

Figure 8 shows the FTIR spectra of the extruded samples as well as the raw protein powder. The amide I peak ($\approx 1640\text{ cm}^{-1}$) of the raw protein powder is marked in the figures as a dashed line. Compared to the raw 75Z powder spectrum, it can be observed that the 75Z extrudate and HOx extrudate spectra are slightly shifted toward higher wavenumbers. Shifts to higher wavenumbers indicate larger fractions of unordered random-coil protein structures (e.g., α -helices), while shifts to lower values are associated with more ordered structures (e.g., β -sheets). The shifts are slightly larger for the samples containing HOx, thus indicating more unordered structures as interactions involved hinder more ordered protein structures [32, 33]. The same trends can be observed in Figure 8b,c for the RM extrudate spectra, with the highest shifts relative to the raw protein spectrum occurring for the extrudates containing RM. The shifts are especially apparent for the extrudates based on the 75WG protein blend (Figure 8c). In the context of protein hydrogels produced in the presence of metal ions, more random coil structures (shifts to higher wavenumbers) were related to stronger interactions between the proteins and metal ions in the gel [33]. Thus, the

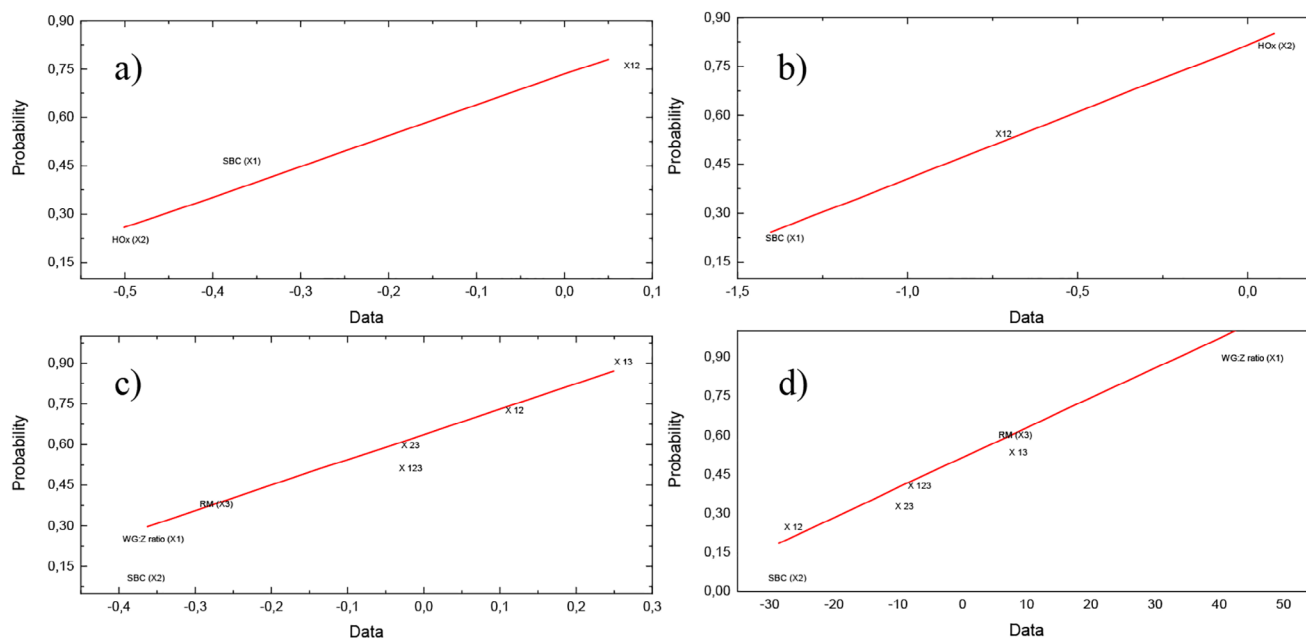


FIGURE 7 | Parameter effects of the maximum (a) tensile stress and (b) strain for extrudates in the HOx experimental design, and maximum (c) tensile stress and (d) strain for extrudates in the RM experimental design.

additional shifts observed in the spectra for HOx and RM indicate changes in protein secondary structure and evidence a protein network characterized by more chain entanglements. This is also in agreement with the rheology and mechanical testing results, suggesting HOx and RM contribute to plasticizing and physical crosslinking, yielding more entangled, flexible (increased chain mobility), and fluid foams.

Peaks around 1720 cm^{-1} are associated with carboxylic acid groups. In the case of the HOx foams, absorbance is expected in this region to a certain extent due to the presence of oxalic acid. However, for the samples containing RM, absorbance in this region could be related to hydrolysis. The peaks are more marked in the spectra for the 75WG/RM foams (Figure 8c).

Future work should explore advanced characterization techniques to build on the FTIR analysis and unveil the role of RM in modifying the chemical structure of the protein-based foam, such as in-situ temperature FTIR, solid-state NMR and Dynamic Mechanical Analysis (DMA) on the extruded material.

3.3 | SDS Extractability (Estimation of Crosslinking Degree)

SDS extracts were prepared from extrudates to assess protein crosslinking, where higher SDS extractability indicates reduced crosslinking. SDS-PAGE analysis revealed distinct soluble protein size distributions, reflecting the influence of extrudate composition on cross-linking. The study examined the effect of sodium bicarbonate (SBC) to the following formulations: 75Z/HOx, 75WG/RM, and 75Z/RM. The SDS-extractable protein fractions correspond to wheat gluten and zein, providing insights into their solubility and interactions during extrusion. Variability in

molecular weight may arise from crop-specific factors such as variety, growth conditions, or crop year [50].

In Figure 9, high molecular weight glutenins ($\approx 100\text{ kDa}$) in most samples, forming polymeric structures crucial for the gluten network. Monomeric gliadins (70–25 kDa) are also present, contributing to wheat gluten's viscoelasticity: ω -gliadins (55–70 kDa) influence viscosity, γ -gliadins (35–40 kDa) enhance structural integrity, and α -/ β -gliadins (25–35 kDa) promote extensibility and cohesiveness [51]. Protein signals at 20–25 kDa correspond to α -zein, the predominant fraction in zein isolates, contributing to hydrophobicity and film formation [52]. Bands $\approx 15\text{ kDa}$ indicate smaller hydrolyzed protein fragments, likely resulting from partial degradation of wheat gluten and zein during extrusion [53].

HOx leachate samples exhibit well-defined protein bands corresponding to wheat gluten and zein fractions. Soluble proteins extracted at 20–25 kDa (α -zein) and 35–40 kDa (γ -gliadins) suggest incomplete crosslinking, while a weaker signal at $\approx 100\text{ kDa}$ indicates high molecular weight glutenins. Both samples show qualitatively similar protein profiles, but differences in signal intensity suggest that SBC influences the crosslinking degree in the zein-dominant oxalic acid protein network. This correlates with mechanical properties, as SBC-containing 75Z blends exhibit lower stress and Young's modulus, indicating a weaker, less cohesive structure.

In the case of the red mud-containing samples, they exhibit prominent protein bands, particularly for α -zeins and γ -gliadins, indicating incomplete crosslinking: the incorporation of this multivalent ionic material (such as Fe^{3+} and Al^{3+}) introduces metal-protein co-ordinations with the protein functional groups [33, 54, 55]. In gluten, this coordination may interfere with disulfide bond formation, while in zein, glutamine-rich regions

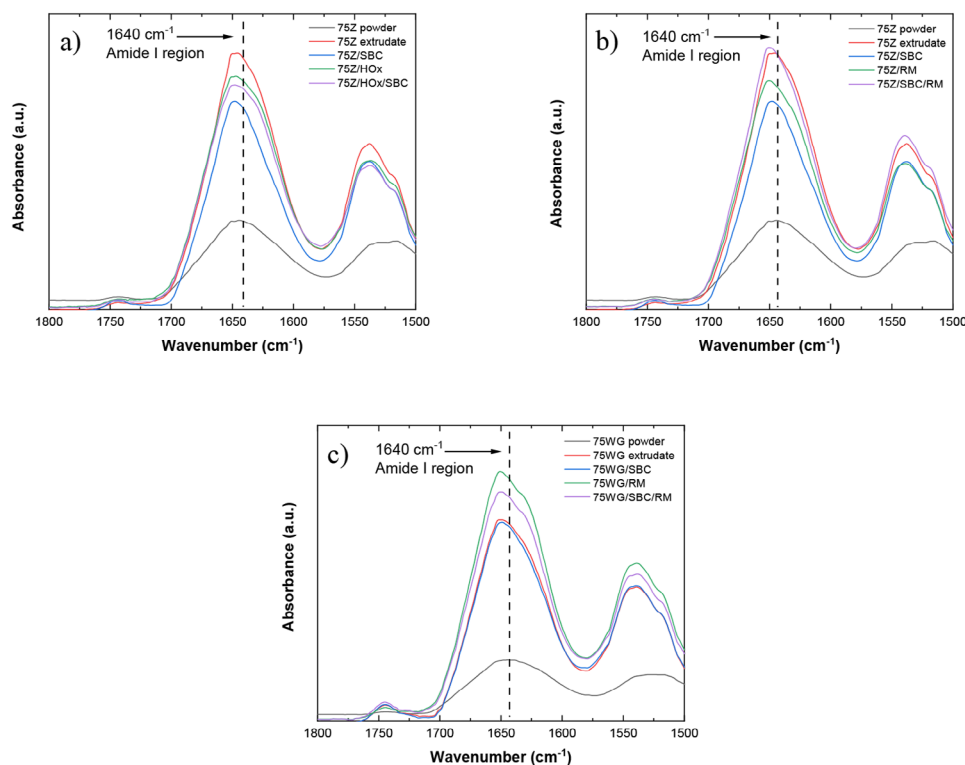


FIGURE 8 | FTIR spectra for (a) HOx and references, (b) RM and reference systems based on the 75Z protein blend, and (c) RM and reference systems based on the 75WG/ protein blend. The frequency range is limited to contain the Amide I peak as well as a potential carboxylic acid peak for hydrolysis detection.

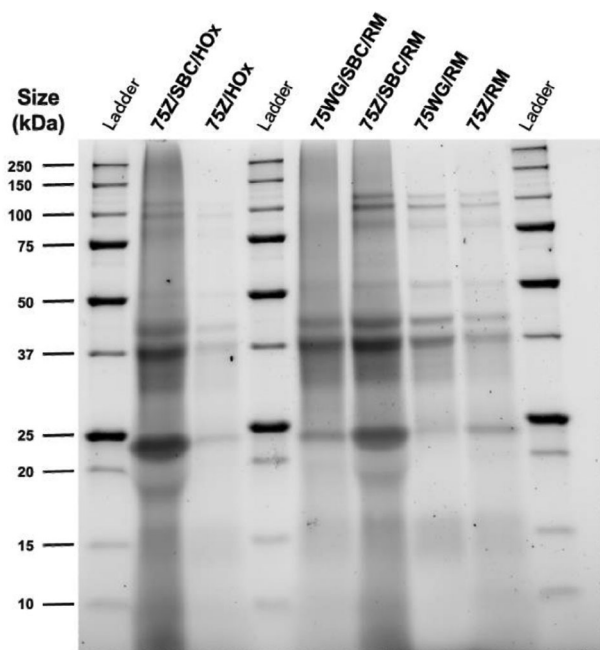


FIGURE 9 | SDS-PAGE fractions of the SDS-extractable protein from the different formulations.

can disrupt the helical structure, promoting conformational changes as manifested by FTIR spectra. These signals are slightly stronger than in HOx formulations, suggesting that red mud, irrespective of the wheat gluten/zein ratio, may hinder crosslinking

in these fractions, altering the mechanical properties. Indeed, the mechanical analysis confirm this behavior, as RM-containing foams show increased strain but lower Young's modulus, indicating a plasticizing rather than reinforcing effect. This effect is most pronounced in 75Z/SBC/RM, where stronger protein band intensities suggest reduced protein network stability, a trend similar to the observed in oxalic acid formulations.

In 75WG/SBC/RM sample, the absence of high molecular weight glutenins (≈ 100 kDa) suggests enhanced crosslinking within the protein matrix compared to the SBC-free counterpart. This aligns with mechanical results showing a higher expansion ratio, lower density (increased porosity), and reduced Young's modulus, leading to greater brittleness. In this case, SBC may promote glutenin crosslinking in gluten-dominant formulations by modifying pH or facilitating disulfide bond formation [56, 57]. However, this effect appears inconsistent, as 75Z/SBC/RM sample exhibits detectable wheat gluten bands at ≈ 100 kDa. This suggests that SBC's ability to promote glutenin crosslinking is more pronounced when gluten is the dominant protein in the extrudate formulation but less effective when zein predominates.

4 | Conclusion

This study explored the utilization of red mud, a significant solid waste from alumina production, as an additive in the extrusion of foams derived from wheat gluten and zein, which are by-products of the agricultural industry. Two forms of red mud were assessed: oxalic acid leachate (HOx), produced through acid leaching of red

mud powder, and raw red mud powder (RM). Adding HOx did not significantly alter foam densities, while RM notably decreased the density in the high gluten blend with sodium bicarbonate, correlating with an open porous structure and high absorption capacity. Rheological analyses showed that HOx reduced initial storage modulus and moduli disparity post-glass transition while slightly increasing storage moduli, indicating roles as a plasticizer and crosslinking agent. Conversely, the inclusion of RM substantially increased storage modulus values, indicative of enhanced crosslinking and potential oxidizing effects. These rheological trends were corroborated by tensile tests, which showed that both HOx and RM reduced stress and Young's modulus, while RM notably increased the strain of the 75WG foam to 190%. This indicates a less rigid and dense network with increased chain mobility between proteins, consistent with a more plasticized matrix potentially containing long crosslinks. Changes were also observed in protein secondary structures, favoring more random coil formations potentially due to plasticizing effects and metal-protein interactions. Consequently, HOx and RM act as an additive, enhancing flexibility while impeding stiffness. Therefore, applications should leverage their ability to accommodate elastic deformations under low load rather than requiring rigid, stable structures.

Acknowledgements

The authors thank FORMAS (BioRESorb project, grant 2022-00362) and Vinnova via the ERA-NET Cofund on Raw Materials (ERA-MIN3) program ("Abtomat—Utilization Of Aluminum Bearing Raw Materials For The Production Of Aluminum Metal, Other Metals, And Compounds", grant 2021-05201). The authors would like to thank ETI Aluminum for the samples.

Conflicts of Interest

The authors declare no conflicts of interest.

Data Availability Statement

The data that support the findings of this study are available from the corresponding author upon reasonable request.

References

1. R. Chandrappa and D. B. Das, *Solid Waste Management: Principles and Practice* (Springer, 2012).
2. V. Yadav and S. Shrotriya, *Waste-To-Wealth: Resource Recovery and Value-Added Products for Sustainable Development* (CRC Press, 2024).
3. M. Ram and E. Bracci, "Waste Management, Waste Indicators and the Relationship With Sustainable Development Goals (SDGs): A Systematic Literature Review," *Sustainability* 16 (2024): 8486.
4. S. Salazar Sandoval, A. Amenábar, I. Toledo, N. Silva, and P. Contreras, "Advances in the Sustainable Development of Biobased Materials Using Plant and Animal Waste as Raw Materials: A Review," *Sustainability* 16 (2024): 1073, <https://doi.org/10.3390/su16031073>.
5. X. Li, T. Zhang, G. Lv, K. Wang, and S. Wang, "Summary of Research Progress on Metallurgical Utilization Technology of Red Mud," *Minerals* 13 (2023): 737.
6. N. C. G. Silveira, M. L. F. Martins, A. C. S. Bezerra, and F. G. S. Araújo, "Red Mud From the Aluminum Industry: Production, Characteristics, and Alternative Applications in Construction Materials—a Review," *Sustainability* 13 (2021): 12741.

7. M. A. Khairul, J. Zanganeh, and B. Moghtaderi, "The Composition, Recycling and Utilization of Bayer Red Mud," *Resources, Conservation and Recycling* 141 (2019): 483–498.
8. B. Swain, A. Akcil, and J.-C. Lee, "Red Mud Valorization An Industrial Waste Circular Economy Challenge; Review Over Processes and Their Chemistry," *Critical Reviews in Environmental Science and Technology* 16 (2022): 520–570, <https://doi.org/10.1080/10643389.2020.1829898>.
9. C. R. Borra, Y. Pontikes, K. Binnemans, and T. Van Gerven, "Leaching of Rare Earths From Bauxite Residue (Red Mud)," *Minerals Engineering* 76 (2015): 20–27.
10. S. Rai, S. Bahadure, M. J. Chaddha, and A. Agnihotri, "Disposal Practices and Utilization of Red Mud (Bauxite Residue): A Review in Indian Context and Abroad," *Journal of Sustainable Metallurgy* 6 (2020): 1–8.
11. S. Rai, S. Bahadure, M. J. Chaddha, and A. Agnihotri, "Disposal Practices and Utilization of Red Mud (Bauxite Residue): A Review in Indian Context and Abroad," *Journal of Sustainable Metallurgy* 6 (2020): 1–8.
12. S. Gao, B. Song, S. Wang, J. Vaughan, Z. Zhu, and H. Peng, "A Low-Cost Process for Complete Utilization of Bauxite Residue," *Journal of Environmental Management* 356 (2024): 120751.
13. D. Avdibegović, M. Regadio, and K. Binnemans, "Efficient Separation of Rare Earths Recovered By a Supported Ionic Liquid from Bauxite Residue Leachate," *RSC Advance* 8 (2018): 11886–11893.
14. A. Svobodova-Sedlackova, et al., "Mapping the Research Landscape of Bauxite By-Products (Red Mud): An Evolutionary Perspective from 1995 to 2022," *Heliyon* 10 (2024).
15. E. Mukiza, L. Zhang, X. Liu, and N. Zhang, "Utilization of Red Mud in Road Base and Subgrade Materials: A review," *Resources, Conservation and Recycling* 141 (2019): 187–199, <https://doi.org/10.1016/j.resconrec.2018.10.031>.
16. S. Samal, "Utilization of Red Mud as a Source for Metal Ions—A Review," *Materials* 14 (2021): 2211, <https://doi.org/10.3390/ma14092211>.
17. M. Archambo and S. K. Kawatra, "Red Mud: Fundamentals and New Avenues for Utilization," *Mineral Processing and Extractive Metallurgy Review* 42 (2021): 427–450.
18. D. V. Zinoveev, V. G. Diubanov, A. V. Shutova, and M. V. Ziniaeva, "Recycling of Red Muds With the Extraction of Metals and Special Additions to Cement," *Russian Metallurgy (Metally)* 2015 (2015): 19–21.
19. K. Evans, "The History, Challenges, and New Developments in the Management and Use of Bauxite Residue," *Journal of Sustainable Metallurgy* 2 (2016): 316–331.
20. X. Liu, Y. Han, F. He, P. Gao, and S. Yuan, "Characteristic, Hazard and Iron Recovery Technology of Red Mud—A Critical Review," *Journal of Hazardous Materials* 420 (2021): 126542, <https://doi.org/10.1016/j.jhazmat.2021.126542>.
21. C. R. Borra, B. Blanpain, Y. Pontikes, K. Binnemans, and T. Van Gerven, "Recovery of Rare Earths and Other Valuable Metals from Bauxite Residue (Red Mud): A Review," *Journal of Sustainable Metallurgy* 2 (2016): 365–386.
22. D. Avdibegović, M. Regadio, and K. Binnemans, "Efficient Separation of Rare Earths Recovered By a Supported Ionic Liquid from Bauxite Residue Leachate," *RSC Advance* 8 (2018): 11886–11893.
23. R. A. Pepper, S. J. Couperthwaite, and G. J. Millar, "Comprehensive Examination of Acid Leaching Behavior of Mineral Phases from Red Mud: Recovery of Fe, Al, Ti, and Si," *Minerals Engineering* 99 (2016): 8–18.
24. C. R. Borra, Y. Pontikes, K. Binnemans, and T. Van Gerven, "Leaching of Rare Earths From Bauxite Residue (Red Mud)," *Minerals Engineering* 76 (2015): 20–27.
25. Y. Yang, X. Wang, M. Wang, H. Wang, and P. Xian, "Recovery of Iron From Red Mud by Selective Leach With Oxalic Acid," *Hydrometallurgy* 157 (2015): 239–245.

26. I. Ghosh, S. Guha, R. Balasubramaniam, and A. V. R. Kumar, "Leaching of Metals From Fresh and Sintered Red Mud," *Journal of Hazardous Materials* 185 (2011): 662–668.
27. Starch Europe. The European starch industry, Available at: starch.eu/the-european-starch-industry/ (2024).
28. H. Zabed, J. N. Sahu, A. Suely, A. N. Boyce, and G. Faruq, "Bioethanol Production From Renewable Sources: Current Perspectives and Technological Progress," *Renewable and Sustainable Energy Reviews* 71 (2017): 475–501.
29. A. J. Capezza, R. Mezzenga, "Proteins for Applied and Functional Materials," *Biomacromolecules* 25, (2024): 4615–4618, <https://doi.org/10.1021/acs.biomac.4c00884>.
30. C. E. Federico, Q. Wu, R. T. Olsson, and A. J. Capezza, "Three-dimensional (3D) Morphological and Liquid Absorption Assessment of Sustainable Biofoams Absorbents Using X-ray Microtomography Analysis," *Polymer Testing* 116 (2022): 107753.
31. A. J. Capezza, M. Bettelli, X. Wei, M. Jiménez-Rosado, A. Guerrero, and M. Hedenqvist, "Biodegradable Fiber-Reinforced Gluten Biocomposites for Replacement of Fossil-Based Plastics," *ACS Omega* 9 (2024): 1341–1351.
32. M. A. Bettelli, A. J. Capezza, F. Nilsson, E. Johansson, R. T. Olsson, and M. S. Hedenqvist, "Sustainable Wheat Protein Biofoams: Dry Upscalable Extrusion at Low Temperature," *Biomacromolecules* 23 (2022): 5116–5126.
33. X. Ye, A. J. Capezza, X. Xiao, et al., "Protein Nanofibrils and Their Hydrogel Formation With Metal Ions," *ACS Nano* 15 (2021): 5341–5354.
34. L. B. Hurtado Colmenares, M. Nejati, Y. Fang, et al., "New Sources of Genipin-Rich Substances for Crosslinking Future Manufactured Bio-Based Materials," *RSC Sustainability* 2 (2023): 125–138.
35. A. Jugé, J. Moreno-Villafranca, V. M. Perez-Puyana, M. Jiménez-Rosado, M. Sabino, and A. J. Capezza, "Porous Thermoformed Protein Bioblends as Degradable Absorbent Alternatives in Sanitary Materials," *ACS Applied Polymer Materials* 5 (2023): 6976–6989.
36. A. J. Capezza, E. Robert, M. Lundman, et al., "Extrusion of Porous Protein-based Polymers and Their Liquid Absorption Characteristics," *Polymers (Basel)* 12 (2020): 459.
37. A. J. Capezza, M. Lundman, R. T. Olsson, W. R. Newson, M. S. Hedenqvist, and E. Johansson, "Carboxylated Wheat Gluten Proteins: A Green Solution for Production of Sustainable Superabsorbent Materials," *Biomacromolecules* 21 (2020): 1709–1719.
38. Y. Wang, Y. Zhang, J. Du, et al., "A Novel Iron Ion Cross-linking Strategy Dramatically Improves the Strength and Flame Retardant of Degradable Foams From Rice Straw Fibers," *Advanced Composites Hybrid Mater* 8 (2025): 11.
39. F. H. Arnold and J. Zhang, "Metal-Mediated Protein Stabilization," *Trends in Biotechnology* 12 (1994): 189.
40. Y. Chen, P. G. Miller, X. Ding, C. E. T. Stowell, K. M. Kelly, and Y. Wang, "Chelation Crosslinking of Biodegradable Elastomers," *Advanced Materials* 32 (2020): 2003761.
41. J. A. Rufián-Henares, S. Pastoriza, Maillard Reaction, In *Encyclopedia of Food and Health* (2016): 593–600. <https://doi.org/10.1016/B978-0-12-384947-2.00435-9>.
42. H. Pan, X. Xu, B. Jiang, J. Chen, and Z. Jin, "Effect of the Extent and Morphology of Phase Separation on the Thermal Behavior of co-blending Systems Based on Soy Protein Isolate/Alginate," *Food Hydrocolloids* 52 (2016): 393–402.
43. F. L. Jara, A. M. R. Pilosof, "Glass Transition Temperature of Protein/Polysaccharide Co-Dried Mixtures as Affected by the Extent and Morphology of Phase Separation," *Thermochimica Acta* 487 (2009): 65–73.
44. N. K. Budhavaram, J. A. Miller, Y. Shen, and J. R. Barone, "Protein Substitution Affects Glass Transition Temperature and Thermal Stability," *Journal of Agricultural and Food Chemistry* 58 (2010): 9549–9555.
45. M. Pouplin, A. Redl, and N. Gontard, "Glass Transition of Wheat Gluten Plasticized With Water, Glycerol, or Sorbitol," *Journal of Agricultural and Food Chemistry* 47 (1999): 538–543.
46. G. Attenburrow, D. J. Barnes, A. P. Davies, and S. J. Ingman, "Rheological Properties of Wheat Gluten," *Journal of Cereal Science* 12 (1990): 1–14.
47. A. P. C. Duarte, et al. Determination of the Temperature-Dependent Thermophysical Properties of Polymeric Foams Using Numerical Inverse Analysis, *Construction and Building Materials* 394, (2023): 131980.
48. J. Y. Cha, D. S. Chung, P. A. Seib, R. A. Flores, and M. A. Hanna, "Physical Properties of Starch-Based Foams as Affected by Extrusion Temperature and Moisture Content," *Industrial Crops and Products* 14 (2001): 23–30, www.elsevier.com.
49. L. B. Hurtado, M. Jiménez-Rosado, M. Nejati, et al., "Genipap Oil as a Natural Cross-Linker for Biodegradable and Low-Ecotoxicity Porous Absorbents via Reactive Extrusion," *Biomacromolecules* 25 (2024): 7642–7659, <https://doi.org/10.1021/acs.biomac.4c00883>.
50. M. Nadeem, F. M. Anjum, M. R. Khan, M. Sajjad, S. Hussain, and M. S. Arshad, "Electrophoretic Characteristics of Gluten Proteins as Influenced by Crop Year and Variety," *International Journal of Food Properties* 19 (2016): 897–910.
51. H. Wieser, P. Koehler, and K. A. Scherf, "Chemistry of Wheat Gluten Proteins: Qualitative Composition," *Cereal Chemistry* 100 (2023): 23–35.
52. Y. Zhang, W. Li, R. Lan, and J. Y. Wang, "Quality Monitoring of Porous Zein Scaffolds: A Novel Biomaterial," *Engineering* 3 (2017): 130–135.
53. K. Shi, J. L. Kokini, and Q. Huang, "Engineering Zein Films With Controlled Surface Morphology and Hydrophilicity," *Journal of Agricultural and Food Chemistry* 57 (2009): 2186–2192.
54. J. Bjorksten, "Cross Linkages in Protein Chemistry," *In Advances in Protein Chemistry* 6 (1951), 343.
55. D. Teng, Y. Xu, T. Zhao, X. Zhang, Y. Li, and Y. Zeng, "Zein Adsorbents With Micro/Nanofibrous Membrane Structure for Removal of Oils, Organic Dyes, and Heavy Metal Ions in Aqueous Solution," *Journal of Hazardous Materials* 425 (2022): 128004.
56. K. J. A. Jansens, B. Lagrain, K. Brijs, B. Goderis, M. Smet, and J. A. Delcour, "Impact of Acid and Alkaline Pretreatments on the Molecular Network of Wheat Gluten and on the Mechanical Properties of Compression-Molded Glassy Wheat Gluten Bioplastics," *Journal of Agricultural and Food Chemistry* 61 (2013): 9393–9400.
57. S. Garg, M. J. Cran, and V. K. Mishra, "Effect of Heating and Acidic pH on Characteristics of Wheat Gluten Suspension," *International Journal of Food Science and Technology* 54 (2019): 1892–1900.

Supporting Information

Additional supporting information can be found online in the Supporting Information section.

Supporting file 1: mame70039-sup-0001-SuppMat.docx